arXiv:0911.4820v1 [astro-ph.CO] 25 Nov 2009

Constraint on Coupled Dark Energy Models from Observations

Jun-Qing Xia*
Scuola Internazionale Superiore di Studi Avanzati, Via Beirut 2-4, I-34014 Trieste, Italy

The coupled dark energy models, in which the quintessence scalar field nontrivially couples to the cold dark matter, have been proposed to explain the coincidence problem. In this paper we study the perturbations of coupled dark energy models and the effects of this interaction on the current observations. Here, we pay particular attention to its imprint on the late-time Integrated Sachs-Wolfe (ISW) effect. We perform a global analysis of the constraints on this interaction from the current observational data. Considering the typical exponential form as the interaction form, we obtain that the strength of interaction between dark sectors is constrained as $\beta < 0.085$ at 95% confidence level. Furthermore, we find that future measurements with smaller error bars could improve the constraint on the strength of coupling by a factor two, when compared to the present constraints.

PACS numbers: 98.80.Cq, 98.80.-k

I. INTRODUCTION

Current cosmological observations, such as the cosmic microwave background (CMB) measurements of temperature anisotropies and polarization [1] and the redshift-distance measurements of Type Ia Supernovae (SNIa) at $z < 2$ [2], have demonstrated that the Universe is now undergoing an accelerated phase of expansion and that its total energy budget is dominated by the dark energy component. The nature of dark energy is one of the biggest unsolved problems in modern physics and has been extensively investigated in recent years, both under the theoretical and the observational point of view.

The simplest candidate of dark energy is the cosmological constant, where the equation of state w always remains -1. In the standard Λ-Cold Dark Matter (ΛCDM) cosmology, cold dark matter only interacts with other components by gravity, while dark energy is simply a cosmological constant without any evolution and perturbation. Although this concordance model can fit the current observational data very well [1, 2], the possibility of dynamical dark energy models cannot be ruled out yet. Furthermore, this model suffers of the fine-tuning and coincidence problems, i.e. why the Universe is dominated by dark energy in late times [3, 4].

In order to lift these severe tensions, many alternative dynamical dark energy models, such as quintessence [5, 6, 7, 8], phantom [9], K-essence [10, 11] and quintom [12], have been proposed recently (for a review see Ref.[13]). For example, the quintessence model, a scalar field ϕ slowly rolling down a potential energy $V(\phi)$, has the spatial fluctuations and its equation of state w_ϕ can evolve with the cosmic time. More importantly, being a dynamical component, the quintessence is naturally expected to interact with the other components, such as the cold dark matter [14, 15] or massive neutrinos [16, 17], in the field theory framework. If these interactions really exist, it would open up the possibility of detecting the dark energy non-gravitationally.

In the coupled dark energy models, the quintessence scalar field could nontrivially couple to the cold dark matter component. The presence of the interaction clearly modifies the cosmological background evolutions. The evolution of cold dark matter energy density $\rho_c(a)$ will be different, when compared to that of the minimally coupled models, and dependent on the quintessence field ϕ:

$$\rho_{\rm c}(a) = \rho_{\rm c0} a^{-3+\delta(\phi)} , \quad (1)$$

where a is the scale factor, $\rho_{\rm c0}$ is the present value of cold dark matter energy density, and $\delta(\phi)$ is the modification due to the interactions and could be non-zero during the evolution of Universe. In this case, at early times there will be more (less) cold dark matter energy density, when $\delta(\phi) < 0$ (> 0).

On the other hand, the interaction between dark sectors will also affect the evolution of cosmological perturbations, which has been widely investigated recently (see e.g. Refs.[18, 19, 20, 21, 22, 23, 24, 25, 26, 27, 28]). Due to the different evolution of cold dark matter energy density, the interaction between dark sectors could shift the matter-radiation equality scale factor $a_{\rm eq}$, and affect the locations and amplitudes of acoustic peaks of CMB temperature anisotropies and the turnover scales of large scale structure (LSS) matter power spectrum consequently. In addition, the interaction will also affect the late ISW effect [29] at large scales which is produced by the CMB photons passing through the time-evolving gravitational potential well, when dark energy or curvature becomes important at later times [23, 30].

Therefore, with the accumulation of observational data and the improvements of the data quality, it is of great interest to investigate the non-minimally coupled dark energy models from the current observational data. In this paper we study the perturbations of coupled dark energy models and present the constraints on the interactions from the observational data in detail. The structure of the paper is as follows: in Sec.II and Sec.III we show the basic equations of background evolution and linear perturbations of the coupled dark energy model, respectively. In Sec.IV we present the current and future observational datasets we used. Sec.V contains our main global fitting results from the current and future observations, while Sec.VI is dedicated to the summary.

---

*Electronic address: xia@sissa.it

II. BACKGROUND EVOLUTION

In our analysis we assume a flat, homogeneous, Friedmann-Robertson-Walker universe with metric

$$ds^2 = a^2(\eta)\left(-d\eta^2 + dx_i dx^i\right) \ , \tag{2}$$

where η is the conformal time. The Friedmann equation is:

$$\mathcal{H}^2 \equiv \left(\frac{\dot{a}}{a}\right)^2 = \frac{8\pi G}{3} a^2 \rho_{\rm tot} \ , \tag{3}$$

where $\rho_{\rm tot}$ is the total energy density of Universe and the dot refers to the derivative with respect to the conformal time η.

From the Lagrangian of the quintessence scalar field:

$$\mathcal{L}_\phi = \frac{1}{2}\partial_\mu\phi\,\partial^\mu\phi - V(\phi) \ , \tag{4}$$

we can obtain the energy density and pressure

$$\rho_\phi = \frac{\dot{\phi}^2}{2a^2} + V(\phi) \ , \quad p_\phi = \frac{\dot{\phi}^2}{2a^2} - V(\phi) \ . \tag{5}$$

And the Friedmann equation Eq.(3) becomes:

$$\mathcal{H}^2 = \frac{8\pi G}{3} a^2 \left(\rho_\gamma + \rho_{\rm b} + \rho_{\rm c} + \frac{\dot{\phi}^2}{2a^2} + V(\phi)\right) \ , \tag{6}$$

where ρ_γ, $\rho_{\rm b}$ and $\rho_{\rm c}$ are the energy densities of radiation, baryons and cold dark matter, respectively. Consequently, we define the energy density parameters $\Omega_{\rm i} \equiv \rho_{\rm i}/\rho_{\rm tot}$, where $\rho_{\rm i}$ is the energy density of each component. In the following calculations we will set the reduced Planck mass $M_{\rm pl} = 1/\sqrt{8\pi G} \equiv 1$.

Here, we consider the typical exponential form as the quintessence potential, namely

$$V(\phi) = V_0 e^{-\lambda\phi} \ . \tag{7}$$

We also take the exponential form:

$$\rho_{\rm c}(\phi) = \rho_{\rm c}^* e^{\beta\phi} \ , \tag{8}$$

as the interaction form between quintessence and cold dark matter, where $\rho_{\rm c}^*$ is the bare energy density of cold dark matter and β is the strength of interaction. There are several stringent constrains on this strength of interaction, namely, $|\beta| \lesssim \mathcal{O}(0.1)$ at 95% confidence level, from different observations [24, 31, 32]. Using these potential forms, the initial choice of $\phi_{\rm i}$ will not affect the evolution of Universe significantly. And this coupled model could be reduced to the standard ΛCDM model by choosing $\lambda = \beta = 0$ straightforwardly. The effective potential of this coupled system is given by: $V_{\rm eff}(\phi) = V(\phi) + \rho_{\rm c}(\phi)$. If we restrict to the case $\lambda > 0$, this effective potential will have a minimal value at $\phi_{\rm min} = \ln(\lambda V_0/\beta\rho_{\rm c})/\lambda$ for the strength $\beta > 0$. Therefore, in our following calculations we will restrict the forms to the case $\lambda > 0$ and $\beta > 0$ to lead to the acceleration expansion of Universe at late times.

When including the interactions, the conservation of energy momentum for each component becomes [23]:

$$T^\mu_{\nu;\mu} = \beta\phi_{,\nu} T^\alpha_\alpha \ . \tag{9}$$

In our analysis, we assume that the baryons and radiation are not coupled with the quintessence scalar field. Therefore, when considering the interaction between cold dark matter and quintessence, the energy conservation equations of CDM and quintessence will be violated, while those of baryons and radiation are held:

$$\begin{aligned}
\dot{\rho}_\gamma + 4\mathcal{H}\rho_\gamma &= 0 \ , && (10)\\
\dot{\rho}_{\rm b} + 3\mathcal{H}\rho_{\rm b} &= 0 \ , && (11)\\
\dot{\rho}_{\rm c} + 3\mathcal{H}\rho_{\rm c} &= Q_{\rm c} = \beta\dot{\phi}\rho_{\rm c} \ , && (12)\\
\dot{\rho}_\phi + 3\mathcal{H}\rho_\phi(1 + w_\phi) &= Q_\phi = -\beta\dot{\phi}\rho_{\rm c} \ , && (13)
\end{aligned}$$

where the energy exchange $Q_{\rm c}$ is the function of ϕ. When $Q_{\rm c} < 0$ (> 0), the energy of cold dark matter (dark energy) transfers to dark energy (cold dark matter). Because we describe the dark energy component using a quintessence scalar field, the energy conservation equation Eq.(13) will be describe as the Klein-Gordon equation:

$$\ddot{\phi} + 2\mathcal{H}\dot{\phi} + a^2 V'(\phi) = -a^2\beta\rho_{\rm c} \ , \tag{14}$$

where the prime denotes the derivative with respect to the quintessence scalar field ϕ: $V'(\phi) \equiv \partial V(\phi)/\partial\phi$.

We can also define the effective equation of state of CDM and quintessence field to describe the equivalent uncoupled model in the background:

$$\begin{aligned}
\dot{\rho}_{\rm c} + 3\mathcal{H}\rho_{\rm c}(1 + w_{\rm c}^{\rm eff}) &= 0 \ , && (15)\\
\dot{\rho}_\phi + 3\mathcal{H}\rho_\phi(1 + w_\phi^{\rm eff}) &= 0 \ , && (16)
\end{aligned}$$

where the effective equation of state are given by:

$$w_{\rm c}^{\rm eff} = -\frac{\beta\dot{\phi}}{3\mathcal{H}} \ , \quad w_\phi^{\rm eff} = w_\phi + \frac{\beta\dot{\phi}}{3\mathcal{H}}\frac{\rho_{\rm c}}{\rho_\phi} \ . \tag{17}$$

We can find that in this case the effective equation of state of cold dark matter $w_{\rm c}^{\rm eff}$ will be non-vanishing and evolves with the cosmic time.

Based on these equations, we can study the background evolutions of each component in the non-minimal coupling system. In Fig.1 we illustrate the evolutions of

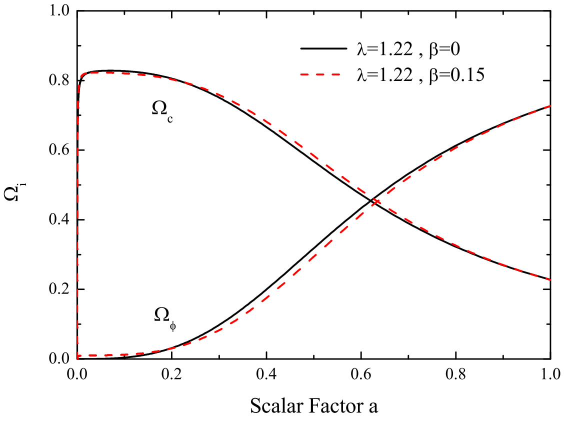

FIG. 1: The cosmological evolutions of the cold dark matter and quintessence energy density parameters, $\Omega_{\rm i}$, for two models: $\lambda = 1.22$, $\beta = 0$ (black solid lines) and $\lambda = 1.22$, $\beta = 0.15$ (red dashed lines).

the cold dark matter and quintessence energy density parameters as a function of redshift for two different models: the uncoupled model $\lambda = 1.22$, $\beta = 0$ (black solid lines) and the coupled system $\lambda = 1.22$, $\beta = 0.15$ (red dashed lines). For other cosmological parameters, we fix them to the best fit values of WMAP5 data [1]: $\Omega_{\rm b}h^2 = 0.02267$, $\Omega_{\rm c}h^2 = 0.1131$, and $h = 0.705$. Here, we normalize energy density parameters to their present values.

Clearly, the interaction between the quintessence scalar field and the cold dark matter significantly modifies the evolutions of their energy density. Because of the presence of the coupling, during the evolution, $\beta\dot{\phi} < 0$ and the energy density of cold dark matter evolves faster than a^{-3}. Therefore, if we normalize energy density parameters to their present values, the cold dark matter energy density will be larger than that of the uncoupled model. The energy of cold dark matter transfers to dark energy.

III. LINEAR PERTURBATION

In this section we will consider the evolution of cosmological perturbations in the non-minimally coupled quintessence model. Starting from the metric in the synchronous gauge [33, 34, 35], the line element is given by:

$$ds^2 = -a^2(\eta)\left(-d\eta^2 + (\delta_{ij} + h_{ij})dx^i dx^j\right) \ , \tag{18}$$

where h_{ij} is the metric perturbation in this synchronous coordinate system. Here, we restrict only for the scalar mode of the metric perturbations.

We write the inhomogeneous energy density of cold dark matter and the quintessence scalar field as:

$$\begin{aligned}\rho_{\rm c}(\eta,\vec{x}) &= \rho_{\rm c}(\eta) + \delta\rho_{\rm c}(\eta,\vec{x}) \\ &= \rho_{\rm c}(\eta)(1+\delta_{\rm c}(\eta,\vec{x})) \ , &(19)\\ \phi(\eta,\vec{x}) &= \phi(\eta) + \delta\phi(\eta,\vec{x}) \ , &(20)\end{aligned}$$

where $\rho_{\rm c}(\eta)$ and $\phi(\eta)$ are the background parts, while $\delta\rho_{\rm c}$ and $\delta\phi$ are the perturbations. Using the perturbed part of the energy momentum conservation equation Eq.(9) for the coupled system, we could calculate the evolution equations for the perturbation of cold dark matter:

$$\begin{aligned}\dot{\delta}_{\rm c} &= 3(\mathcal{H} + \beta\dot{\phi})\left(w_{\rm c} - \frac{\delta p_{\rm c}}{\delta\rho_{\rm c}}\right)\delta_{\rm c} - (1+w_{\rm c})\left(\theta_{\rm c} + \frac{\dot{h}}{2}\right) \\ &\quad + \beta(1-3w_{\rm c})\delta\dot{\phi} + \beta'\dot{\phi}\,\delta\phi(1-3w_{\rm c}) \ , &(21)\\ \dot{\theta}_{\rm c} &= -\mathcal{H}(1-3w_{\rm c})\theta_{\rm c} - \frac{\dot{w_{\rm c}}}{1+w_{\rm c}}\theta_{\rm c} + \frac{\delta p_{\rm c}/\delta\rho_{\rm c}}{1+w_{\rm c}}k^2\delta_{\rm c} \\ &\quad + \beta\frac{1-3w_{\rm c}}{1+w_{\rm c}}k^2\delta\phi - \beta(1-3w_{\rm c})\dot{\phi}\theta_{\rm c} - k^2\sigma_{\rm c} \ , &(22)\end{aligned}$$

where $\delta p_{\rm c}$ is the pressure perturbation of cold dark matter, h is the metric perturbation, $\theta_{\rm c} = ik_j v_{\rm c}^j$ is the gradient of the velocity field, and $\sigma_{\rm c}$ is the shear stress of cold dark matter. In our coupling form Eq.(8), β is a constant, so we have $\beta' \equiv \partial\beta/\partial\phi = 0$. Finally we obtain the perturbation equations of cold dark matter:

$$\begin{aligned}\dot{\delta}_{\rm c} &= -\theta_{\rm c} - \dot{h}/2 + \beta\delta\dot{\phi} \ , &(23)\\ \dot{\theta}_{\rm c} &= -\mathcal{H}\theta_{\rm c} - \beta\dot{\phi}\theta_{\rm c} + k^2\beta\delta\phi \ . &(24)\end{aligned}$$

We note that in the presence of interaction, the gradient of the velocity $\theta_{\rm c}$ will evolve to be nonzero, even if its initial value is zero; whereas $\theta_{\rm c}$ remains zero at all times in the minimally coupled model. Therefore, in our calculations we will evolve the perturbation equations in an arbitrary synchronous gauge, instead of the cold dark matter rest frame [24].

Meanwhile, the perturbed Klein-Gordon equation is given by:

$$\delta\ddot{\phi} + 2\mathcal{H}\delta\dot{\phi} + k^2\delta\phi + a^2V''\delta\phi + \dot{h}\dot{\phi}/2 = -a^2\beta\rho_{\rm c}\delta_{\rm c} \ . \tag{25}$$

We find that the perturbations of this non-minimally coupled system are stable. This is different from some coupling models in which dark energy component is modelled as a fluid with constant equation of state parameter w. In those models, when w is close to the cosmological constant boundary, the coupling term $Q \sim \rho_{\rm c}$ will lead to an instability [26, 27, 28, 36].

In this paper we still choose the adiabatic initial condition, which implies that the entropy perturbation between cold dark matter and quintessence:

$$\mathcal{S} = \frac{\delta\rho_{\rm c}}{\rho_{\rm c}} - \frac{\delta\rho_\phi}{\rho_\phi} = 0 \ , \tag{26}$$

and the quintessence intrinsic entropy perturbation:

$$\mathcal{I} = \frac{\delta\rho_\phi}{\rho_\phi} - \frac{\delta p_\phi}{p_\phi} = 0 \ , \tag{27}$$

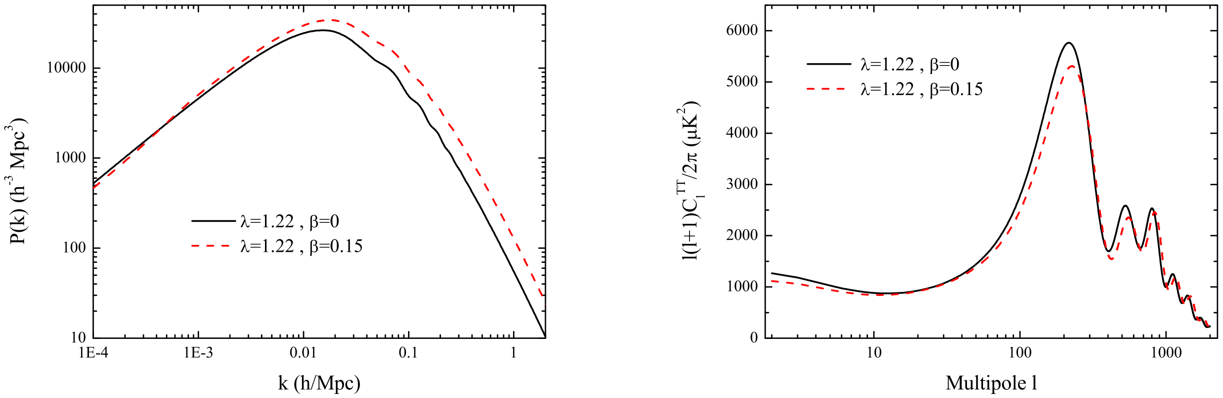

FIG. 2: The CMB temperature anisotropies and LSS matter power spectrum for two models: $\lambda = 1.22$, $\beta = 0$ (black solid lines) and $\lambda = 1.22$, $\beta = 0.15$ (red dashed lines).

vanish at early times. However, during the evolution of Universe, the iso-curvature perturbations will be produced and the adiabatic condition is generally no longer conserved, even for large-scale modes, due to the presence of non-minimal coupling [26, 28].

Following the above equations, we modify the `CAMB` code [37] to calculate the CMB temperature power spectrum $C_\ell^{\rm TT}$ and LSS matter power spectrum $P(k)$ in this non-minimal coupling scenario. Besides the background parameters, we also set $\tau = 0.084$, $n_{\rm s} = 0.96$ and $A_{\rm s} = 2.15 \times 10^{-9}$ at $k = 0.05\,{\rm Mpc}^{-1}$, which are the best fit values obtained from the WMAP5 data [1].

In Fig.2 we plot the CMB temperature power spectrum and LSS matter power spectrum for two different models. In this non-minimally coupled system the matter power spectrum is almost unchanged and the growth of density perturbations are not affected significantly on the large scales [21]. However, on the small scales the situation will be different. As we mentioned before, at early times there is higher cold dark matter energy density in the coupled model with $\beta > 0$. In this case, the epoch of equality $a_{\rm eq}$ occurs further from the recombination. An earlier $a_{\rm eq}$ means only the very small scale modes enter the horizon and decay during the radiation dominated epoch. Therefore, the amplitude of small scale matter power spectrum is enhanced and the turnover occurs on the smaller scales as shown in the left panel of Fig.2. Consequently, the expected value of σ_8 will become larger than that of the minimally coupled case.

In the CMB temperature power spectrum, the most obvious effect is that the amplitude on the small scales has been decreased significantly due to the presence of interaction between dark sectors. In the non-minimally coupled model, the epoch of equality $a_{\rm eq}$ occurs further from the recombination, so that at recombination the inhomogeneities induced from the radiation becomes small. The small-scale anisotropies decrease when the coupling strength is increasing. In addition, the locations of the acoustic peaks in the CMB temperature anisotropies will also slightly shifted to the smaller scales, due to the presence of interaction.

More interestingly, the non-minimal coupling $\beta > 0$ also suppresses the anisotropies on the large scales ($\ell < 20$) which arise mainly from the late-time ISW effect. When β is positive, the energy transfers from cold dark matter to dark energy and at early times cold dark matter density becomes larger. Consequently, the dark matter-dark energy equality scale factor $a'_{\rm eq}$ will be larger than that of the un-coupled case. Because the gravitational potential Φ stays constant in the matter dominated era, $\dot{\Phi}$ and additional CMB anisotropies at large scales will be suppressed in the presence of non-minimal coupling. The CMB temperature anisotropies on very large scales become small, as shown in Fig.2. Therefore, observing the late time ISW effect could be a helpful way of studying the nontrivially coupling between dark sectors.

However, the most significant ISW effect contributes to the CMB anisotropies on large scales that are strongly affected by the cosmic variance. Fortunately, this problem can be solved by the cross-correlation between ISW temperature fluctuation and the density of astrophysical objects like galaxies or quasars. (For the details, we refer the reader to Refs.[38, 39, 40].) In Fig.3 we plot the cross-correlation power spectra C_ℓ^{gT} for two different models using the public package `CAMB_sources`[1]. One can find that the power spectrum C_ℓ^{gT} of the non-minimal coupling case will also be suppressed. The non-minimal coupling leaves an interesting imprint on the cross correlation power spectrum. We expect that the observational ISW data could improve the constraints on the interac-

---

[1] Available at http://camb.info/sources/.

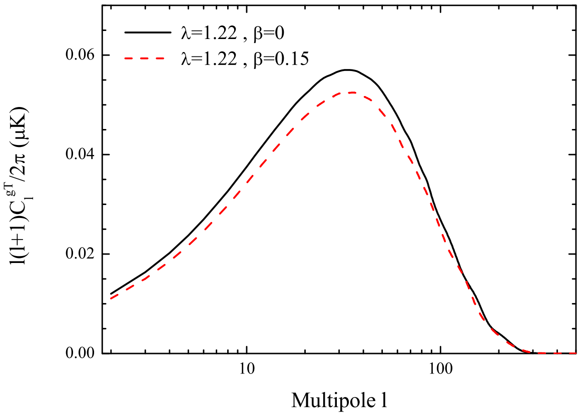

FIG. 3: The cross-correlation signal C_ℓ^{gT} for two models: $\lambda = 1.22$, $\beta = 0$ (black solid lines) and $\lambda = 1.22$, $\beta = 0.15$ (red dashed lines).

tion.

IV. OBSERVATIONAL DATA

A. Current Datasets

In our calculations, we will rely here on the following cosmological probes: i) CMB anisotropies and polarization; ii) baryonic acoustic oscillations in the galaxy power spectra; iii) SNIa distance moduli; and iv) the angular auto-correlation (ACF) and cross-correlation (CCF) functions data obtained from the quasar map and CMB map.

In the computation of CMB power spectra we have included the WMAP five-year (WMAP5) temperature and polarization power spectra with the routines for computing the likelihood supplied by the WMAP team [1, 41, 42, 43, 44, 45]. Since the non-minimal coupling also leaves some signatures on the small scales CMB power spectrum, in our calculations we also include some small-scale CMB measurements to improve the constraints, such as BOOMERanG [46], CBI [47] and ACBAR [48].

BAOs (Baryonic Acoustic Oscillations) have been detected in the current galaxy redshift survey data from the SDSS and the Two-degree Field Galaxy Redshift Survey (2dFGRS) [49, 50, 51, 52]. The BAO can directly measure not only the angular diameter distance, $D_A(z)$, but also the expansion rate of the universe, $H(z)$, which is powerful for studying dark energy [53]. Since current BAO data are not accurate enough for extracting the information of $D_A(z)$ and $H(z)$ separately [54], one can only determine an effective distance [49]:

$$D_v(z) \equiv \left[(1+z)^2 D_A^2(z)\frac{cz}{H(z)}\right]^{1/3} . \tag{28}$$

In this paper we use the Gaussian priors on the distance ratios $r_s(z_d)/D_v(z)$:

$$\begin{aligned} r_s(z_d)/D_v(z=0.20) &= 0.1980 \pm 0.0058 , \\ r_s(z_d)/D_v(z=0.35) &= 0.1094 \pm 0.0033 , \end{aligned} \tag{29}$$

with a correlation coefficient of 0.39, extracted from the SDSS and 2dFGRS surveys [52], where r_s is the comoving sound horizon size and z_d is drag epoch at which baryons were released from photons given by Ref.[55].

The SNIa data provide the luminosity distance as a function of redshift which is also a very powerful measurement of cosmological evolution. The supernovae data we use in this paper are the recently released Union compilation (307 samples) from the Supernova Cosmology project [2], which include the recent samples of SNIa from the (Supernovae Legacy Survey) SNLS and ESSENCE survey, as well as some older data sets, and span the redshift range $0 \lesssim z \lesssim 1.55$. In the calculation of the likelihood from SNIa we have marginalized over the nuisance parameter as done in Ref.[56].

For the observational ISW data, we use the ACF and CCF data obtained from the quasar map of Sloan Digital Sky Survey Data Release Six [57] and the WMAP5 Internal Linear Combination (ILC) map [41], which has been used in Ref.[58]. (Also, Refs.[59, 60] provided the observational ISW data using different CMB and LSS surveys.) This ISW data set gives the information at very low redshift ($z \sim 1$) which is much lower than the recombination ($z \sim 1100$). Thus, we do not consider the possible covariance matrix between this ISW data and the WMAP power spectra C_ℓ.

Furthermore, we make use of the Hubble Space Telescope (HST) measurement of the Hubble parameter $H_0 \equiv 100\,h$ km s^{-1} Mpc^{-1} by a Gaussian likelihood function centered around $h = 0.72$ and with a standard deviation $\sigma = 0.08$ [61].

B. Future Datasets

In order to forecast future measurements we will use the same observables as before without BAO.

For the simulation with Planck [62], we follow the method given in Ref.[63] and mock the CMB temperature (TT) and polarization (EE) power spectra and temperature-polarization cross-correlation (TE) with the isotropic noise by assuming a given fiducial cosmological model. In Table I, we list the assumed experimental specifications of the future (mock) Planck measurement. Here we neglect foregrounds and the tensor information. The effective χ^2 is:

$$\chi^2_{\rm eff} \equiv -2\log\mathcal{L}$$

TABLE I. Assumed experimental specifications for the mock Planck-like measurements. The noise parameters Δ_T and Δ_P are given in units of μK-arcmin.

$f_{\rm sky}$	$\ell_{\rm max}$	(GHz)	$\theta_{\rm fwhm}$	Δ_T	Δ_P
0.65	2500	100	9.5'	6.8	10.9
		143	7.1'	6.0	11.4
		217	5.0'	13.1	26.7

$$= \sum_{\ell}(2\ell+1)\left\{\log\left(\frac{C_\ell^{TT}C_\ell^{EE}-(C_\ell^{TE})^2}{\tilde{C}_\ell^{TT}\tilde{C}_\ell^{EE}-(\tilde{C}_\ell^{TE})^2}\right)\right. \quad (30)$$

$$\left. + \frac{\tilde{C}_\ell^{TT}C_\ell^{EE}+C_\ell^{TT}\tilde{C}_\ell^{EE}-2\tilde{C}_\ell^{TE}C_\ell^{TE}}{C_\ell^{TT}C_\ell^{EE}-(C_\ell^{TE})^2}-2\right\} ,$$

where C_ℓ^{XY} denote theoretical power spectra and $\tilde{C}_\ell^{XY}$ denote the power spectra from the simulated data. The gaussian likelihood function has been normalized with respect to the maximum likelihood, where $C_\ell^{XY}=\tilde{C}_\ell^{XY}$ [64, 65].

The proposed satellite SNAP (Supernova / Acceleration Probe) will be a space based telescope with a one square degree field of view that will survey the whole sky [66]. It aims at increasing the discovery rate of SNIa to about 2000 per year in the redshift range $0.2<z<1.7$. In this paper we simulate about 2000 SNIa according to the forecast distribution of the SNAP [67]. For the error, we follow the Ref.[67] which takes the magnitude dispersion to be 0.15 and the systematic error $\sigma_{\rm sys}=0.02\times z/1.7$. The whole error for each data is given by $\sigma_{\rm mag}(z_i)=\sqrt{\sigma^2_{\rm sys}(z_i)+0.15^2/n_i}$, where n_i is the number of supernovae of the i'th redshift bin. Here, we do not consider the possible covariance matrix among these redshift bins.

For the future ISW ACF and CCF data, we simulate the mock dataset from the best fit values of current data combination CMB+BAO+SNIa+ISW. We reduce the error bars of these data points by a factor three. We also use directly the covariance matrix taken from present data and divide it by a factor nine. This improvement could be achievable by next generation of large-scale surveys such as the Large Synoptic Survey Telescope (LSST, [68]), the Panoramic Survey Telescope and Rapid Response System (Pan-STARRS, [69]) and the Dark Energy Survey (DES; The Dark Energy Survey Collaboration 2005). These surveys are likely to allow for an order of magnitude improvement in the number of quasars, which account for the factor three considered here if we assume that the error bars scale as $\sqrt{N_{\rm quasar}}$. Also, the coverage of the sky fraction is at present of the order of 20% by SDSS DR6, so an all-sky survey will already give a factor two improvement. Another possible improvement in this direction is the use of type-2 quasars instead of the type-1 used here that could further decrease the error bars of the sample (see the discussion in Ref.[57]).

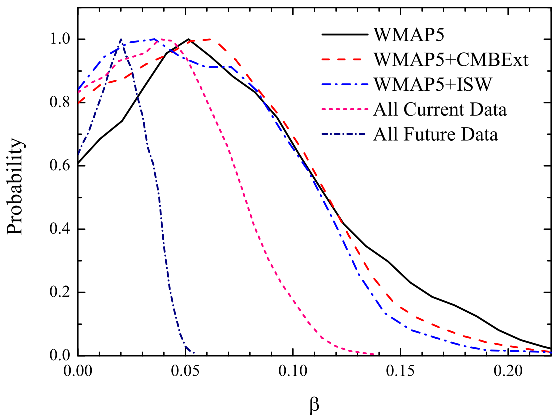

FIG. 4: One dimensional posterior distributions of the strength of interaction β from various data combinations: WMAP5 alone (black solid line), WMAP5+CMBExt (red dashed line), WMAP5+ISW (blue dash-dot line), all current data sets (magenta short dashed line), and all future data sets (navy blue short dash-dot line).

V. NUMERICAL RESULTS

In our analysis, we perform a global fitting using the `CosmoMC` package [70] a Monte Carlo Markov Chain (MCMC) code, which has been modified to calculate the theoretical ACF and CCF. We assume purely adiabatic initial conditions and a flat universe, with no tensor contribution. Besides the parameters λ and β in the potential and coupling forms, we also vary the following cosmological parameters with top-hat priors: the dark matter energy density $\Omega_{\rm c}h^2\in[0.01,0.99]$, the baryon energy density $\Omega_{\rm b}h^2\in[0.005,0.1]$, the primordial spectral index $n_{\rm s}\in[0.5,1.5]$, the primordial amplitude $\log[10^{10}A_{\rm s}]\in[2.7,4.0]$ and the angular diameter of the sound horizon at last scattering $\theta\in[0.5,10]$. For the pivot scale we set $k_{\rm s0}=0.05\,{\rm Mpc}^{-1}$. When CMB data are included, we also vary the optical depth to reionization $\tau\in[0.01,0.8]$. We do not consider any massive neutrino contribution. From the parameters above the MCMC code derives the reduced Hubble parameter H_0, the present matter fraction $\Omega_{\rm m0}$, and σ_8, so, these parameters have non-flat priors and the corresponding bounds must be interpreted with some care. There are three more parameters related to the ACF and CCF data: the constant bias b, the efficiency of quasar catalog a and the ISW amplitude $A_{\rm amp}$ which is defined by: $\bar{C}^{\rm qT}(\theta)=A_{\rm amp}C^{\rm qT}(\theta)$, where $\bar{C}^{\rm qT}$ and $C^{\rm qT}$ are the observed and theoretical CCF. In addition, `CosmoMC` imposes a weak prior on the Hubble parameter: $h\in[0.4,1.0]$.

In Fig.4 we show the one-dimensional posterior distributions of β from various data combinations. Firstly, we present the constraint from the WMAP5 data alone (black solid line). For the strength of interaction, the constraint is still weak, namely the 95% upper limit is $\beta < 0.165$, which is consistent with other results in the literature [24, 31, 32]. As we mentioned before, the non-minimal coupling shifts the acoustic peaks of CMB temperature anisotropies on the small scales. The small-scale CMB measurements (CMBExt) should improve the constraints on the coupling strength. Therefore, we plot the constraint on β from WMAP5+CMBExt data combination in Fig.4 (red dashed line). When adding the small-scale CMB data, we can find that the constraint on β improves slightly: $\beta < 0.135$ at 95% confidence level. The small-scale CMB observations indeed improve the constraint.

We also include the observational ISW data [58] into our calculations. In Fig.4 we show the one dimensional distribution of β from WMAP5+ISW data combination (blue dash-dot line). We can find that the combined constraint from WMAP5+ISW is slightly improved over using WMAP5 alone, namely, the 95% upper limit of the coupling strength is $\beta < 0.130$. Since at present constraints from the ISW data are still very weak and in the calculations we only consider the high-redshift quasar catalog and totally neglect other low-redshift tracers which could give powerful ISW constraints [59, 60], the constraint on β does not improve significantly. When combining WMAP5, CMBExt and ISW data together, the constraint on β will improve further: $\beta < 0.120$ at 95% confidence level.

Finally we combine all the current datasets together to constrain the coupling strength β. In Fig.4 we find that the constraint tightens significantly (magenta short dashed line):

$$\beta < 0.050 \ (0.085) \tag{31}$$

at 68% (95%) confidence level. The 95% upper limit is reduced by a factor of 2, when compared to the constraint from WMAP5 alone, which is due to the constraining power of SNIa and BAO on the evolutions of cosmological background parameters. Meanwhile, the parameter λ in the potential form of quintessence scalar field is constrained to be $\lambda < 1.05$ at 95% confidence level, which is consistent with the result in Ref.[24].

As we mentioned before, the non-minimal coupling ($\beta > 0$) affects the large scale structure formation. From Fig.2 we can see that the matter power spectrum on the small scales will be enhanced significantly by the large value of β. The positive β will lead to a high value of σ_8 today. Using the all datasets combination, we obtain the limit on σ_8 today of $\sigma_8 = 0.816 \pm 0.040$ (68% C.L.), which is obviously higher than one obtained in the minimally coupled model ($\beta = 0$): $\sigma_8 = 0.793 \pm 0.030$ (68% C.L.), while the error bar is enlarged slightly. Therefore, the σ_8 today and β are correlated as we expected, as shown the black solid lines in Fig.5.

In Fig.6 we also show the two dimensional contour in the (λ, β) panel. When λ is larger than zero, the equation of state of dark energy will evolve with cosmic time, and the dark energy acts more like the dark matter ($w_\phi > -1$). In this case the dark energy will dominate our Universe at relatively higher redshift and slow down the linear growth function of the matter perturbation and leads to a low value of σ_8 today. The constraint of $\sigma_8 = 0.793 \pm 0.030$ (68% C.L.) from all current datasets is obviously lower than that of the pure ΛCDM: $\sigma_8 = 0.812 \pm 0.026$ (68% C.L.) [1]. As the parameter λ increases, in order to reach the same value of σ_8 today, the strength of coupling β should be increased at the same time. Therefore, λ and β are also correlated, illustrated in Fig.6.

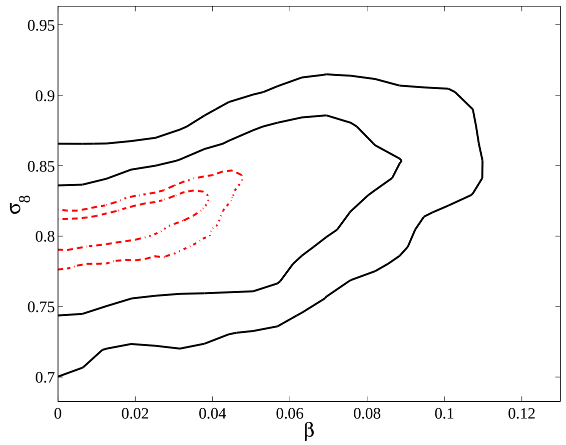

FIG. 5: Two dimensional marginalized contour in the (β, σ_8) panel from all current data sets (black solid lines) and all future data sets (red dash-dot lines), respectively.

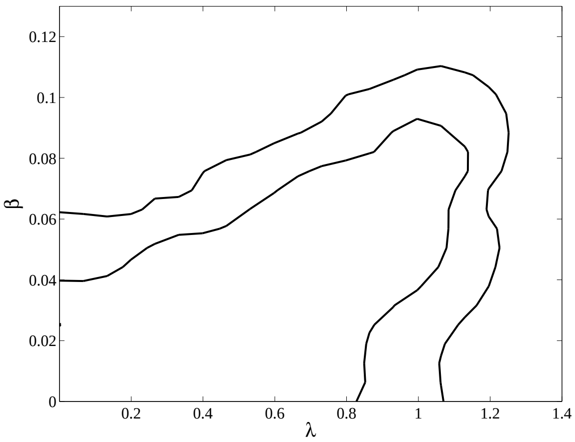

FIG. 6: Two dimensional marginalized contour in the (λ, β) panel from all current data sets combination.

From the results presented above, we can see the current observations could give the constraints on the strength of interaction as $\beta < \mathcal{O}(0.1)$ at 95% confidence level. It is worthwhile to discuss whether future data could give more stringent constraints on β.

Therefore, in Fig.4 we also present the constraint on the strength of interaction β from the future datasets (navy blue short dash-dot line). Due to the smaller error bars of the mock data sets, the constraint on β improves significantly, namely the 68% (95%) upper limits are now

$$\beta < 0.025\ (0.039)\ , \tag{32}$$

which are reduced by another factor of 2, when compared to the current constraint Eq.(31). We also show the two dimensional contour in the (β, σ_8) panel (red dash-dot lines) in Fig.5. The correlation still exists and the limits have been shrunk significantly. These results imply that the future measurements could constrain the non-minimal coupled dark energy model with a higher precision.

VI. SUMMARY

The coupled dark energy models, in which the quintessence scalar field non-minimally couples to the cold dark matter, could affect the CMB temperature anisotropies and LSS matter power spectrum. In this paper we present constraints on this coupled dark energy model using the latest observations and future measurements. The WMAP5 data alone could only give a weak constraint on the strength of coupling β. And then we exploit the capabilities of the late-time ISW effect in constraining the non-minimal coupling, using the cross-correlation signal between the quasar sample of SDSS DR6 [57] and the WMAP5 ILC map [41]. We find that the current ISW data could slightly improve the constraint on β. If we add the BAO and SNIa data into our calculations, the constraint on β will improves significantly, namely the 95% upper limit is $\beta < 0.085$. Finally we simulate the future measurements with smaller error bars and find that the future measurements could improve the constraint on the strength of coupling by a factor of two, when compared to the present constraints.

---

[1] E. Komatsu *et al.*, Astrophys. J. Suppl. **180**, 330 (2009).
[2] M. Kowalski *et al.*, Astrophys. J. **686**, 749 (2008).
[3] S. Weinberg, Rev. Mod. Phys. **61**, 1 (1989).
[4] I. Zlatev, L. M. Wang and P. J. Steinhardt, Phys. Rev. Lett. **82**, 896 (1999).
[5] R. D. Peccei, J. Sola and C. Wetterich, Phys. Lett. B **195**, 183 (1987).
[6] C. Wetterich, Nucl. Phys. B **302**, 668 (1988).
[7] B. Ratra and P. J. E. Peebles, Phys. Rev. D **37**, 3406 (1988).
[8] P. J. E. Peebles and B. Ratra, Astrophys. J. **325**, L17 (1988).
[9] R. R. Caldwell, Phys. Lett. B **545**, 23 (2002).
[10] T. Chiba, T. Okabe and M. Yamaguchi, Phys. Rev. D **62**, 023511 (2000).
[11] C. Armendariz-Picon, V. F. Mukhanov and P. J. Steinhardt, Phys. Rev. Lett. **85**, 4438 (2000).
[12] B. Feng, X. L. Wang and X. Zhang, Phys. Lett. B **607**, 35 (2005).
[13] E. J. Copeland, M. Sami and S. Tsujikawa, Int. J. Mod. Phys. D **15**, 1753 (2006).
[14] E. J. Copeland, A. R. Liddle, and D. Wands, Phys. Rev. D **57**, 4686 (1998).
[15] L. Amendola, Phys. Rev. D **62**, 043511 (2000).
[16] P. Gu, X. Wang, and X. Zhang, Phys. Rev. D **68**, 087301 (2003).
[17] R. Fardon, A. E. Nelson, and N. Weiner, JCAP **0410**, 005 (2004).
[18] J. C. Hwang and H. Noh, Class. Quant. Grav. **19**, 527 (2002).
[19] L. Amendola, Phys. Rev. D **69**, 103524 (2004).
[20] T. Koivisto, Phys. Rev. D **72**, 043516 (2005).
[21] S. Lee, G. C. Liu, and K. W. Ng, Phys. Rev. D **73**, 083516 (2006).
[22] G. Olivares, F. Atrio-Barandela, and D. Pavon, Phys. Rev. D **74**, 043521 (2006).
[23] A. W. Brookfield, C. van de Bruck, and L. M. H. Hall, Phys. Rev. D **77**, 043006 (2008).
[24] R. Bean, E. E. Flanagan, I. Laszlo, and M. Trodden, Phys. Rev. D **78**, 123514 (2008).
[25] R. Mainini, JCAP **0807**, 003 (2008).
[26] J. Valiviita, E. Majerotto, and R. Maartens, JCAP **0807**, 020 (2008).
[27] J. H. He, B. Wang, and E. Abdalla, Phys. Lett. B **671**, 139 (2009).
[28] S. Chongchitnan, Phys. Rev. D **79**, 043522 (2009).
[29] R. K. Sachs and A. M. Wolfe, Astrophys. J. **147**, 73 (1967).
[30] J. H. He, B. Wang, and P. J. Zhang, arXiv:0906.0677.
[31] L. Amendola, Phys. Rev. Lett. **86**, 196 (2001).
[32] L. Amendola and C. Quercellini, Phys. Rev. D **68**, 023514 (2003).
[33] H. Kodama and M. Sasaki, Prog. Theor. Phys. Suppl. **78**, 1 (1984).
[34] V. F. Mukhanov, H. A. Feldman, and R. H. Brandenberger, Phys. Rep. **215**, 203 (1992).
[35] C. P. Ma and E. Bertschinger, Astrophys. J. **455**, 7 (1995).
[36] M. B. Gavela, D. Hernandez, L. L. Honorez, O. Mena and S. Rigolin, JCAP **0907**, 034 (2009).
[37] A. Lewis, A. Challinor, and A. Lasenby, Astrophys. J. **538**, 473 (2000); URL: http://camb.info/.
[38] H. V. Peiris and D. N. Spergel, Astrophys. J. **540**, 605 (2000).
[39] A. Cooray, Phys. Rev. D **65**, 103510 (2002).
[40] N. Afshordi, Y. S. Loh, and M. A. Strauss, Phys. Rev. D **69**, 083524 (2004).
[41] G. Hinshaw *et al.*, Astrophys. J. Suppl. **180**, 225 (2009);

URL: http://lambda.gsfc.nasa.gov/.
[42] B. Gold *et al.*, Astrophys. J. Suppl. **180**, 265 (2009).
[43] J. Dunkley *et al.*, Astrophys. J. Suppl. **180**, 306 (2009).
[44] E. L. Wright *et al.*, Astrophys. J. Suppl. **180**, 283 (2009).
[45] M. R. Nolta *et al.*, Astrophys. J. Suppl. **180**, 296 (2009).
[46] C. J. MacTavish *et al.*, Astrophys. J. **647**, 799 (2006).
[47] J. L. Sievers *et al.*, arXiv:0901.4540.
[48] C. L. Reichardt *t al.*, Astrophys. J. **694**, 1200 (2009).
[49] D. J. Eisenstein *et al.* Astrophys. J. **633**, 560 (2005).
[50] S. Cole *et al.* Mon. Not. Roy. Astron. Soc. **362**, 505 (2005).
[51] G. Huetsi, Astron. Astrophys. **449**, 891 (2006).
[52] W. J. Percival *et al.*, Mon. Not. Roy. Astron. Soc. **381**, 1053 (2007).
[53] A. Albrecht *et al.*, arXiv:astro-ph/0609591.
[54] T. Okumura, T. Matsubara, D. J. Eisenstein, I. Kayo, C. Hikage, A. S. Szalay and D. P. Schneider, Astrophys. J. **676**, 889 (2008).
[55] D. J. Eisenstein and W. Hu, Astrophys. J. **496**, 605 (1998).
[56] E. Di Pietro and J. F. Claeskens, Mon. Not. Roy. Astron. Soc. **341**, 1299 (2003).
[57] G. T. Richards *et al.*, Astrophys. J. Suppl. **180**, 67 (2009).
[58] J. Q. Xia *et al.*, arXiv:0907.4753.
[59] T. Giannantonio *et al.*, Phys. Rev. D **77**, 123520 (2008).
[60] S. Ho *et al.*, Phys. Rev. D **78**, 043519 (2008).
[61] W. L. Freedman *et al.*, Astrophys. J. **553**, 47 (2001).
[62] Planck Collaboration, arXiv:astro-ph/0604069.
[63] J. Q. Xia, H. Li, G. B. Zhao and X. Zhang, Int. J. Mod. Phys. D **17**, 2025 (2008).
[64] R. Easther, W. H. Kinney and H. Peiris, JCAP **0505**, 009 (2005).
[65] L. Perotto, J. Lesgourgues, S. Hannestad, H. Tu and Y. Y. Y. Wong, JCAP **0610**, 013 (2006).
[66] URL: http://snap.lbl.gov/.
[67] A. G. Kim, E. V. Linder, R. Miquel and N. Mostek, Mon. Not. Roy. Astron. Soc. **347**, 909 (2004).
[68] J. A. Tyson, in Proc. SPIE 4836, *Survey and Other Telescope Technologies and Discoveries*, ed. J. A. Tyson and S. Wolff (Bellingham, WA: SPIE) (2002).
[69] N. Kaiser *et al.*, in Proc. SPIE 4836, *Survey and Other Telescope Technologies and Discoveries*, ed. J. A. Tyson and S. Wolff (Bellingham, WA: SPIE) (2002).
[70] A. Lewis and S. Bridle, Phys. Rev. D **66**, 103511 (2002); URL: http://cosmologist.info/cosmomc/.